

Statistical mechanics of two-dimensional shuffled foams: prediction of the correlation between geometry and topology

Marc Durand,¹ Jos Käfer,² Catherine Quilliet,³ Simon Cox,⁴ Shirin Ataei Talebi,³ and François Graner⁵

¹*Matière et Systèmes Complexes (MSC), 10 rue Alice Domon et Léonie Duquet, 75205 Paris Cedex 13, France.**

²*Laboratoire de Biométrie et Biologie Evolutive, 43 bd du 11 novembre 1918, 69622 Villeurbanne Cedex, France.†*

³*Laboratoire Interdisciplinaire de Physique, BP 87, 38402 Martin d'Hères Cedex, France.‡*

⁴*Institute of Mathematics and Physics, Aberystwyth University, SY23 3BZ, UK.*

⁵*Polarité, Division et Morphogenèse, Laboratoire de Génétique et Biologie du Développement, Institut Curie, 26 rue d'Ulm, 75248 Paris Cedex 05, France.§*

(Dated: September 5, 2011)

We propose an analytical model for the statistical mechanics of shuffled two-dimensional foams with moderate bubble size polydispersity. It predicts without any adjustable parameters the correlations between the number of sides n of the bubbles (topology) and their areas A (geometry) observed in experiments and numerical simulations of shuffled foams. Detailed statistics show that in shuffled cellular patterns n correlates better with \sqrt{A} (as claimed by Desch and Feltham) than with A (as claimed by Lewis and widely assumed in the literature). At the level of the whole foam, standard deviations Δn and ΔA are in proportion. Possible applications include: correlations of the detailed distributions of n and A ; three-dimensional foams; and biological tissues.

PACS numbers: 83.80.Iz Emulsions and foams, 02.70.Rr General statistical methods

Keywords:

Cellular materials are interesting both as disordered media with well-defined structural elements, and as models for more complex systems such as biological tissues [1]. Among them, foams are ubiquitous in our daily lives and in many industries [2–4]. Bubble monolayers are much easier to observe and to study (Fig. 1). Such quasi two-dimensional foams are characterised by their number of bubbles, N , area distribution, $p(A)$, and number-of-sides distribution, $p(n)$. Their bubbles are polygonal, with shapes that are locally governed by Plateau's laws [3, 4]. Each side is a thin liquid film with a uniform surface tension; its curvature is determined by the difference of pressure between the two bubbles it separates.

Bubble size distribution and packing (or “topology”) are crucial in determining e.g. rheological properties [4]. Statistically, a relatively large bubble, within a given foam sample, has more neighbours than a smaller one. To quantify this intuitive impression, bubbles which have the same number n of neighbours can be grouped, and their normalized average size plotted versus n . One debate [6–15] concerns whether n correlates with A or \sqrt{A} (Fig. 2(a),2(b) and Eqs. (1),(5)). A second debate [11, 12, 14] asks: can we understand these empirical correlations, and prove them; what is their physical origin, and why do they apply only to some cellular patterns? We ask the same questions about empirical observation [16] of proportionality between the *geometrical disorder*, or area polydispersity, $\frac{\Delta A}{\langle A \rangle} = \sqrt{\langle A^2 \rangle - \langle A \rangle^2} / \langle A \rangle$, and the *topological disorder*, $\frac{\Delta n}{\langle n \rangle} = \sqrt{\langle n^2 \rangle - \langle n \rangle^2} / \langle n \rangle$, where $\langle \cdot \rangle$ denotes the average over all bubbles in a foam and Δ the standard deviation (Fig. 2(c)).

Existing models [2, 9, 11, 12, 17–20] seek distributions of n and A which are optimal in some sense. This is rel-

evant at times long enough for $p(A)$ to vary, e.g. under coarsening or bubble coalescence [2–4]. At shorter time scales, N and $p(A)$ are fixed: only the number of sides of the bubbles varies, when they undergo “T1” neighbour changes (Fig. 1d). At most instants the foam is in a local energy minimum, that is, a metastable state; each T1 is instantaneous and followed by a relaxation towards a new local energy minimum [4]. Local minima have almost the same energy, and are separated by high energy barriers corresponding to T1s [18]. There is no process leading towards a global energy minimum. T1s instead induce a random exploration of local minima, effectively “shuffling” the foam [16]. This notion of shuffling is empirically defined [16, 17] as having had enough T1s per bubble to forget about the foam's initial preparation. Numerical simulations and theoretical analyses have shown that cycles of shear of amplitude significantly larger than the yield strain almost completely remove (although seldom perfectly) both residual trapped stresses and spurious correlations [21].

In the present paper, we obtain, for shuffled foams of moderate polydispersity, an *analytical expression* for the distribution of n for *any given distribution* of A . We use a grand-canonical description [22] with a constraint based on mechanical equilibrium and space-filling (the curvature sum rule [2–4]) rather than on energy. Predictions of geometry-topology correlations agree with shuffled foam data obtained from existing experiments on liquid foams [16] and new, refined, numerical simulations of two sorts.

In our experiments (Fig. 1a), a bubble monolayer of up to $N = 2700$ bubbles is confined at the air-water interface by a glass plate [23]. The foam is enclosed in a 324 cm² square with two parallel rigid boundaries (one fixed, one driven by a motor) and two passive lateral

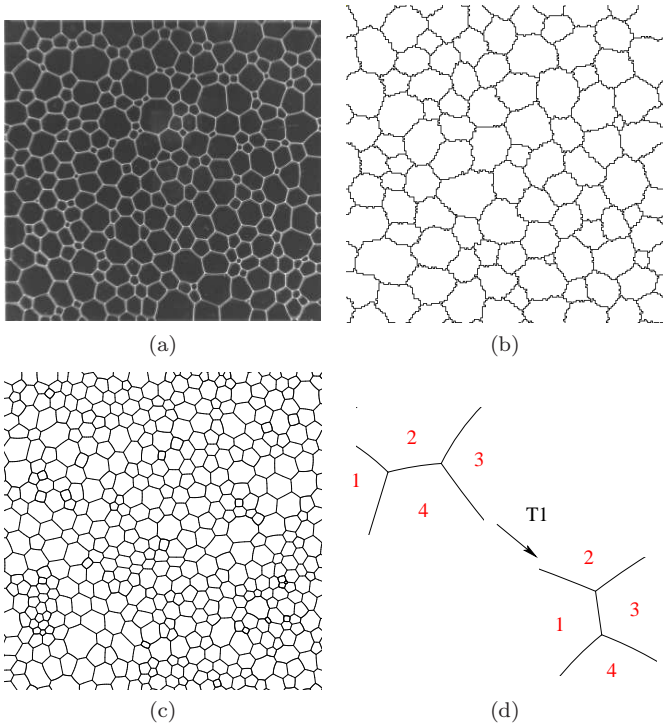


FIG. 1: Examples of shuffled foams. (a) Experiment, after 10 shear cycles. (b) Potts model simulation, after increasing the effective temperature. (c) Surface Evolver simulation, after 10 compression-extension cycles. Monodisperse, bidisperse and polydisperse foams are all generated in both experiments and simulations; only polydisperse foams are shown here. (d) Sketch of a T1 event: bubbles 1 and 3 gain one side, bubbles 2 and 4 lose one; they also exchange some curvature.

boundaries formed by a rubber band [24]. It can thus be deformed into a parallelogram at constant area to apply pure shear cycles with an amplitude much larger than the yield strain. For details see [16, 24].

Potts model simulations [18, 25] (Fig. 1b) are fast, enabling us to scan a large range of disorders and accumulate statistics. They describe each bubble as a set of pixels, like in experimental images. Initially, we distribute at random $N = 112$ nine-pixel bubble seeds on a 200×200 pixel lattice. They are grown until they reach approximately the average bubble size $\langle A \rangle$, chosen to be 400 pixels. They are then randomly assigned target areas according to the desired area distribution. To shuffle the foam, we choose the effective temperature, and thus the amplitude of bubble side fluctuations, high enough that T1s occur spontaneously [1]. The simulations are run for 2×10^6 Monte Carlo Steps (MCS), at which we checked that $\Delta n / \langle n \rangle$ reaches a steady value.

Surface Evolver (SE) [26] simulations represent each side as an arc of a circle (Fig. 1c); they provide detailed information about each bubble's position and shape. Each foam is prepared from a Voronoi construction based on seed points generated by a random Poisson point pro-

cess [27, 28], with the bubble areas adjusted to fit the desired area distribution where necessary, before convergence to an energy minimum. We cyclically shear, by deforming the shape of the periodic box, about four hundred foams with $N = 2500$ bubbles in two perpendicular directions with strain amplitude 1.5.

In experiments and simulations we made bidisperse foams, with the ratio of large to small bubble areas ranging from 1 to 8, and polydisperse foams with normal (Potts), Poisson (SE), or intermediate (experiments) distributions of areas, with relative width $\Delta A / \langle A \rangle$ ranging from 0 to 1.15.

The topology of the foam clearly depends on the relative (and not absolute) bubble sizes. To enable comparisons with simulations and theory, in what follows all data are plotted as dimensionless. We first present averages \bar{n} over individual bubbles. Fig. 2(a) shows the intuitively expected increase of \bar{n} with the bubble size. Moreover, it shows that all simulation data of \bar{n} vs $\sqrt{A} / \langle \sqrt{A} \rangle$ are grouped, and display a *linear* variation, on a much wider range than \bar{n} vs $A / \langle A \rangle$. These ensemble averages require that we bin together bubbles of similar sizes. In addition, in SE simulations we track for each bubble the fluctuations of n with time (A being fixed) and check (not shown here) that time-averages yield exactly the same dependence of \bar{n} on A as ensemble averages.

Second, representations of bubble sizes averaged over bubbles of the same n , without binning, are easy to extract from experiments or simulations, which probably explains their prevalence in the literature [6–12]. Fig. 2(b) shows the intuitively expected increase of $\sqrt{A}(n) / \langle \sqrt{A} \rangle$ with n , but here without obvious superposition of the data; plots (not shown) with bubble perimeter P rather than \sqrt{A} are similar. The fit is *linear*; its slope is very different from the inverse of the slope in Fig. 2(a), due to the statistical character of the relationship between \sqrt{A} (or A) and n [14].

Third, Fig. 2(c) shows measures of the foam's disorder. The topological disorder is *proportional* to the geometrical one up to ~ 0.4 . At higher polydispersity, measures of disorder are less correlated.

Our model for these data is based on the ideas introduced in [22], which we now briefly recall. Each T1 keeps two quantities constant: the sum of n over the four bubbles involved, and the sum of the four bubbles' curvatures κ [5]. A foam's macro-state is thus defined by its total curvature (summed over N bubbles) $\kappa_{tot} = \sum \kappa$ and total number of sides $N_s = \sum n$. Within a macro-state, the set of micro-states is defined as the set of all accessible local energy minima: we assume they all have the same probability, and use a grand-canonical description: consider one particular bubble of area A , the rest of the foam constitutes a reservoir of sides and curvature, exchanged through T1s. We then use a mean field approximation, disregarding neighbour correlations and as-

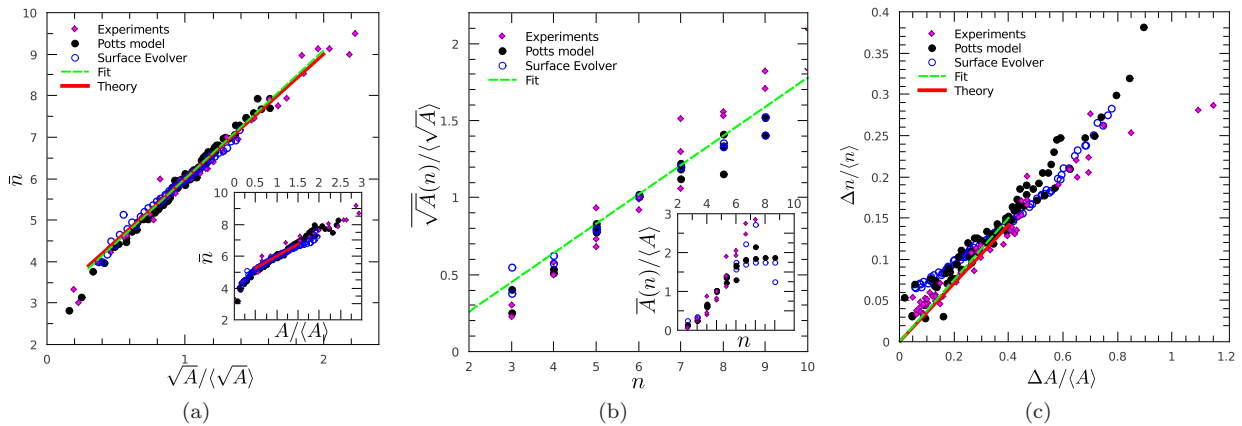


FIG. 2: (color online). Geometry-topology correlations. Purple diamonds: bulk shear experiment; filled black circles: Potts simulations; open blue circles: Surface Evolver simulations. Lines are drawn over the expected range of validity. (a) Average number of sides \bar{n} of a bubble *vs* its relative size $\sqrt{A}/\langle\sqrt{A}\rangle$. Each foam contributes several points: two points for a bidisperse foam, more dispersed points for a polydisperse foam. Green dashed line: linear fit, slope 3.03 ± 0.04 , intercept 2.97 ± 0.04 ; solid red line: Eq. (1). Inset: same data plotted *vs* $A/\langle A \rangle$; solid red line: Eq. (5). (b) Desch-Feltham representation: $\sqrt{A}/\langle\sqrt{A}\rangle$ *vs* n [6–9]. Green dashed line: linear fit, slope 0.19 ± 0.02 , intercept -0.12 ± 0.03 . Inset: Lewis representation, $\bar{A}/\langle A \rangle$ *vs* n [9–12]. (c) Topological *vs* geometrical disorder. Each point represents a foam. Green dashed line: linear fit with zero intercept, slope 0.37 ± 0.03 ; solid red line: Eq. (6).

suming this reservoir foam is homogeneous and isotropic. The probability for a bubble with size A to have n sides is: $p_A(n) = \chi(A)^{-1} e^{-\frac{\pi}{3\bar{e}\sqrt{A}}\beta n(n-6) + \mu n}$, where $\chi(A) = \sum_{n \geq 3} e^{-\frac{\pi}{3\bar{e}\sqrt{A}}\beta n(n-6) + \mu n}$ is the partition function of the bubble. Here $\bar{e} = P/\sqrt{A}$ is close to 3.72 for most bubbles [18]; β^{-1} and $\mu\beta^{-1}$ are analogous to the “temperature” of the reservoir of curvature, and the “chemical potential” of the reservoir of sides, respectively. Their values are unambiguously related to the mean values of κ_{tot} and N_s through $\langle\kappa_{tot}\rangle = -\partial \ln \Xi / \partial \beta$ and $\langle N_s \rangle = \partial \ln \Xi / \partial \mu$, where Ξ is the partition function of the entire foam, defined through $\ln \Xi = N \int_0^\infty p(A) \ln \chi(A) dA$. For a very large foam ($N \rightarrow \infty$), the constraint of space-filling sets the values $\langle\kappa_{tot}\rangle/N \rightarrow 0$ and $\langle N_s \rangle/N \rightarrow 6$ [2, 4, 29]. This (implicitly) relates the distribution of sides $p(n)$ to the distribution of sizes $p(A)$: $p(n) = \int_0^\infty p(A) p_A(n) dA$ [22].

Using the above ideas, we now derive analytical predictions for β and μ , applicable to a foam with small or moderate polydispersity. We first note that $p_A(n)$ can be rewritten as $c(A) e^{-\frac{(n-\bar{n}(A))^2}{2\sigma^2}}$, where $\bar{n}(A) = 3 + 3\bar{e}\mu\sqrt{A}/(2\pi\beta)$, $\sigma^2 = 3\bar{e}\sqrt{A}/(2\pi\beta)$, and $c(A) = \chi(A)^{-1} e^{\frac{\pi\beta\bar{n}^2(A)}{3\bar{e}\sqrt{A}}}$. Thus $p_A(n)$ is a normal distribution. It is truncated at $n \geq 3$ (since there are no 1- or 2-sided bubbles [4]), but if it is narrow enough, $\sigma \ll \bar{n}(A) - 3$, we neglect the effect of such truncation on its integral. We also treat n as a continuous rather than an integer variable. We thus approximate $\bar{n}(A)$ by the mean number of sides of a bubble with area A . Then $\int_0^\infty \bar{n}(A) p(A) dA$ is equal to $\langle n \rangle = 6$, which implies $2\pi\beta\mu^{-1}/\bar{e} = \langle\sqrt{A}\rangle$. We

thus predict and explain the linear variation [13–15]:

$$\bar{n}(A) \simeq 3 \left(1 + \frac{\sqrt{A}}{\langle\sqrt{A}\rangle} \right), \quad (1)$$

which agrees with experimental and numerical data (Fig. 2(a)).

To proceed, we obtain the values of β and μ by solving the system: $\partial \ln \Xi / \partial \mu = 6N$ and $\partial \ln \Xi / \partial \beta = 0$. Still assuming that n varies continuously from $-\infty$ to ∞ , we approximate $c(A)^{-1}$ by the integral $\int_{-\infty}^\infty e^{-\frac{\pi\beta}{3\bar{e}\sqrt{A}}(n-\bar{n}(A))^2} dn$. We obtain the partition function:

$$\chi(A) = \frac{1}{c(A)} e^{\frac{\pi\beta\bar{n}^2(A)}{3\bar{e}\sqrt{A}}} \simeq e^{\frac{\pi\beta\bar{n}^2(A)}{3\bar{e}\sqrt{A}}} \sqrt{\frac{3\bar{e}}{\beta}} A^{1/4}, \quad (2)$$

and then solve for β and μ :

$$\beta^{-1} = \frac{6\pi}{\bar{e}} \left(\langle A^{-1/2} \rangle - \langle A^{1/2} \rangle^{-1} \right), \quad (3)$$

$$\mu^{-1} = 3 \left(\langle A^{1/2} \rangle \langle A^{-1/2} \rangle - 1 \right). \quad (4)$$

We can determine *a posteriori* the domain of validity of neglecting the truncation in n . Using Eqs. (3) and (4), our assumption $\sigma \ll \bar{n}(A) - 3$ requires $A^{1/2}/\langle A^{1/2} \rangle \gg \langle A^{1/2} \rangle \langle A^{-1/2} \rangle - 1$. Thus, the criterion on the width of $p(A)$ is $\langle A^{1/2} \rangle \langle A^{-1/2} \rangle - 1 \ll 1$. It is more intuitive to characterize the width of $p(A)$ by its normalised standard deviation $\frac{\Delta A}{\langle A \rangle}$. For that purpose, we change variable and use the relative deviation ε from monodispersity [30], assumed to be $\ll 1$: the condition of validity of this approximation, and thus of Eq. (1), reduces to $(\Delta A / \langle A \rangle)^2 \ll 4$,

and is thus obeyed by both small and moderate dispersities.

Using the same change of variable, $\bar{n}(A)$ can be expressed as a function of A [30], instead of \sqrt{A} . For foams with a small area dispersity ($\Delta A/\langle A \rangle \ll 1$) we can write:

$$\bar{n}(A) \simeq \frac{3}{2} \left(3 + \frac{A}{\langle A \rangle} \right). \quad (5)$$

The inset of Fig. 2(a) shows the linear variation predicted by Eq. (5). Eqs. (1) and (5) are consistent. As expected, Eq. (1) has a range of validity larger than that of Eq. (5): roughly $A/\langle A \rangle \in [0.16, 2.56]$ vs $[0.50, 1.50]$. Note that we have no simple prediction for the Desch-Feltham or Lewis representation (Fig. 2(b)).

We can also calculate $\Delta n/\langle n \rangle$, using $\langle n^2 \rangle = \int_0^\infty p(A)\chi(A)^{-1} (\partial^2 \chi / \partial \mu^2) dA$ and Eq. (2). This yields $(\Delta n/\langle n \rangle)^2 = [\langle A^{1/2} \rangle \langle A^{-1/2} \rangle + \langle A \rangle \langle A^{1/2} \rangle^{-2} - 2] / 4$. For shuffled foams with a moderate dispersity we obtain [30]:

$$\frac{\Delta n}{\langle n \rangle} \approx \frac{1}{2^{3/2}} \frac{\Delta A}{\langle A \rangle} \approx 0.35 \frac{\Delta A}{\langle A \rangle}. \quad (6)$$

Despite the approximations involved in the analytical derivation of Eq. (6), its prediction is indiscernible from the linear fit to the data over the whole expected range; that is, up to a geometrical disorder of 0.4 (Fig. 2(c)). Note that the agreement is better with experiments than numerics, especially at low disorder. We attribute this small discrepancy to the lower number of bubbles in Potts simulations (~ 2500 bubbles for experiments and SE *versus* 112 for Potts), and to the much lower value of the liquid fraction for SE simulations ($\sim 10^{-3} - 10^{-2}$ for Potts and experiments *versus* $\sim 10^{-5}$ for SE [21]). At larger dispersities the relation between $\Delta n/\langle n \rangle$ and $\Delta A/\langle A \rangle$ depends on the exact shapes of the area distributions: this explains the scatter in the data.

In conclusion, in shuffled two-dimensional foams we predict without any free parameter the correlation between topology and geometry: n correlates better with \sqrt{A} than with A (Eq. (1)), and the two measures of disorder are proportional (Eq. (6)). Although the exact shape of the area distribution plays a role in principle, we expect that in a linear approximation its mean and width play the dominant role. This is what our linear derivation captures. These results should lead to a more accurate description of other shuffled cellular patterns such as some biological tissues and metallic grains, and of shuffling and ergodicity in soft matter.

We thank W. Drenckhan for critical reading of the manuscript, and R. Delannay for providing reference material; F.G. thanks R. de Almeida, P.-L. Bardet, B. Guirao, Y. Bellaïche for discussions; C.Q. and S.A.T. thank P. Ballet and B. Dollet for help with software, and D. Rabaud and S. Riondet for help during experiments. J.K. thanks A.F.M. Marée for help with the Potts simulations. S.C. thanks EPSRC for funding.

-
- * UMR 7057 CNRS & Université Paris Diderot; Electronic address: marc.durand@univ-paris-diderot.fr
- † UMR 5558 CNRS & Université Lyon I
- ‡ UMR 5588 CNRS & Université Grenoble I
- § UMR 3215 CNRS, Inserm U934, UPMC, Curie
- [1] P. Marmottant, A. Mgharbel, J. Käfer, *et al.*, Proc. Nat. Acad. Sci. USA **106**, 17271 (2009).
- [2] D. Weaire and N. Rivier, *Contemp. Phys.*, **25**, 55 (1984).
- [3] S. Hutzler and D. Weaire, “Physics of Foams”, Oxford University Press, Oxford (1999).
- [4] “Les mousses: structure et dynamique”, collective book, Belin, Paris (2010).
- [5] The curvature κ of a bubble is the sum of the algebraic curvatures of its sides, which we count here as positive if the centre of curvature is outside the bubble.
- [6] C.H. Desch, *J. Inst. Met.* **22**, 241 (1919).
- [7] P. Feltham, *Acta Metall.* **5**, 97 (1957).
- [8] K. Y. Szeto and W. Y. Tam, *Physica A* **221**, 256 (1995).
- [9] N. Rivier, in “Disorder and Granular Media”, ed. D. Bideau and A. Hansen, Elsevier, New York (1993), 55.
- [10] F.T. Lewis, *Anat. Rec.* **38**, 341 (1928); *Anat. Rec.* **50**, 235 (1931).
- [11] M. A. Fortes and P. I. C. Teixeira, *J. Phys. A: Math. Gen.* **36**, 5161 (2003).
- [12] G. Schliecker, *Adv. Phys.* **51**, 1319 (2002).
- [13] M. Hillert, *Acta Metall.* **13**, 227 (1965).
- [14] G. Abbruzzese, I. Heckelmann, and K. Lücke, *Acta Metall.* **40**, 519 (1992).
- [15] A. Thorvaldsen, *J. Appl. Phys.* **73** 7839 (1993).
- [16] C. Quilliet, S. Ataei Talebi, D. Rabaud, *et al.*, *Phil. Mag. Lett.* **88** 651 (2008).
- [17] R.M.C. de Almeida and J.R. Iglesias, *J. Phys. A* **21** 3365 (1988); J.R. Iglesias and R.M.C. de Almeida, *Phys. Rev. A* **43** 2763 (1991).
- [18] F. Graner, Y. Jiang, E. Janiaud and C. Flament, *Phys. Rev. E* **63**, 011402 (2000).
- [19] C. Sire and M. Seul, *J. Phys. I France* **5** 97 (1995).
- [20] C. Godrèche, I. Kostov and I. Yekutieli, *Phys. Rev. Lett.* **69** 2674 (1992).
- [21] C. Raufaste, S. J. Cox, P. Marmottant and F. Graner, *Phys. Rev. E* **81**, 031404 (2010).
- [22] M. Durand, *EPL* **90**, 60002 (2010).
- [23] A. Abd el Kader and J.C. Earnshaw, *Phys. Rev. Lett.* **82** 2610 (1999).
- [24] C. Quilliet, M. Idiart, B. Dollet, *et al.*, *Colloids Surf. A* **263**, 95 (2005).
- [25] D.J. Srolovitz, M.P. Anderson, G.S. Grest and P.S. Sahni, *Scr. Metall.* **17**, 241 (1983).
- [26] K. Brakke, *Exp. Math.* **1**, 141 (1992).
- [27] www.susqu.edu/brakke/papers/voronoi.htm.
- [28] S. J. Cox. and E.L. Whittick, *Eur. Phys. J. E* **21**, 49 (2006).
- [29] W.C. Graustein, *Annals of Mathematics* **32**, 149 (1931).
- [30] We use the change of variable $A = \langle A \rangle (1 + \varepsilon)$. Assuming $\varepsilon \ll 1$, we can write any k -th moment of A as an expansion in ε , up to order $O(\langle \varepsilon^3 \rangle)$: $\langle A^k \rangle = \langle A \rangle^k (1 + k(k-1)\langle \varepsilon^2 \rangle/2)$. Thus we obtain: $\langle A^{1/2} \rangle \langle A^{-1/2} \rangle - 1 \simeq \langle \varepsilon^2 \rangle/4$; similarly, $(\Delta A/\langle A \rangle)^2 \simeq \langle \varepsilon^2 \rangle$; and finally $[\langle A^{1/2} \rangle \langle A^{-1/2} \rangle + \langle A \rangle \langle A^{1/2} \rangle^{-2} - 2] / 4 \simeq \langle \varepsilon^2 \rangle/8$.